Argonne NATIONAL LABORATORY

ANL-ART-192

Report on the FY20 Characterization of Age Hardened Alloy 709 Materials

Applied Materials Division

ANL-ART-192

Report on the FY20 Characterization of Age Hardened Alloy 709 Materials

Prepared by

X. Zhang

Nuclear Science and Engineering Division

Argonne National Laboratory

T.–L. Sham

Applied Materials Division

Argonne National Laboratory

August 2020

ABSTRACT

This report provides the results on microstructural characterization of the first commercial heat of Alloy 709 plate material undergone additional age hardening treatment. In FY19, through thermodynamic-kinetic modeling and microstructural characterization, it is determined that the 775°C/10 h age-hardening treatment can promote desired precipitation on dislocations and has the potential to further improve the mechanical performance of the material. In FY20, the treatment protocol was applied to the ESR-1150°C condition, and the microstructure was then compared with the ESR-1100°C condition. It was found that the 1150°C solution annealing (SA) dramatically reduced the dislocation density compared to the 1100°C SA, resulting a smaller number density of Nb-rich fine precipitates which grow on dislocations during the age hardening treatment. Other features are very similar between the two. The effect of age hardening on creep performance is discussed. In addition, TEM characterization of a creep-ruptured sample (600°C/330 MPa) was performed. Specimens from the grip region and the gauge region was studied. The grip region specimen was effectively aged at 600°C for extended period, while the gauge region specimen was mechanically deformed at 600°C. The microstructures are very different, implying the importance of a dynamical effect on precipitation.

TABLE OF CONTENTS

LIST OF TABLES

LIST OF FIGURES

1 Introduction

Advanced materials are a key element in the development of advanced nuclear energy systems. High-performance structural materials allow for a compact and simple design of the reactor structure, and have the potential to reduce the construction and operational costs for the next-generation advanced nuclear reactors. Due to the significant enhancement in time-dependent mechanical properties of the austenitic Alloy 709 relative to 316H stainless steel, a reference construction material for SFR systems, code qualification of Alloy 709 was recommended in FY14. A comprehensive plan for the development of a 500,000-hour, 760°C ASME Code Case and the resolution of structural integrity issues identified by Nuclear Regulatory Commission (NRC) for Alloy 709 was developed in FY15. A Phase I implementation of this plan that includes a 100,000-hour, 650°C ASME code case and the initiation of very long-term creep tests, thermal aging, and sodium exposure of Alloy 709 was established.

Alloy 709 is derived from NF709 (Fe-20Cr-25Ni-1.5Mo-Nb,B,N), which was a commercial heat- and corrosion- resistant austenitic stainless steel developed by Nippon Steel Corporation in Japan for boiler tubing applications. The high strength of NF709 is achieved by controlling the carbon content to 0.07–0.10% and precipitation strengthening by Nb(C,N) (MX phase) and CrNbN (Z phase). NF709 also shows good fabricability properties and weldability. It is regarded as one of the best austenitic steels for elevated temperature applications among commercially-available austenitic alloy classes. The NF709 alloy provides time dependent strength nearly double that for conventional 304 and 316 stainless steels at sodium-cooled fast reactor relevant temperatures (Busby et al 2008). While the cost for this alloy has been estimated at approximately 2-4 times that for 304 SS (and 1.5 to 3 times that for 316 SS), many fossil plants have found that the improved performance outweighs the commodity cost, and is still far below the cost for Ni-based superalloys at comparable strengths. Alloy 709 has the same chemical composition as NF709 but is intended for sodium fast reactor applications that include reactor vessel, core supports, primary and secondary piping, and possibly intermediate heat exchanger and compact heat exchanger. Hence development of processing conditions and fabrication scale up for different product forms such as plates, pipes, bars, forgings and sheets, in addition to seamless tubing, are required.

In FY17, the fabrication scale-up effort was completed for Alloy 709 that was started in FY16. The effort culminated in the procurement of four ingots, totaling about 45,000 lb, that were bottom-poured from the melt by a commercial vendor in September 2016. Three ingots, processed by Argon-Oxygen-Decarburization (AOD), Electroslag Remelting (ESR), and ESR with subsequent Homogenization (ESR-homo) routes, were rolled into plates and each of them were solution annealed at 1050, 1100, and 1150°C. The 9 conditions were subsequently delivered to ANL and ORNL. Several samples were cut from the as-rolled test pieces and solution annealed plates and were analyzed for their microstructures, hardness values, grain sizes, and tensile properties. The results showed that the scaled up heat of Alloy 709 fabricated using commercial practice exhibited tensile properties that exceeded the minimum values specified in the ASME Code Case for commercial heats of NF709 (Natesan, et al. 2017).

In FY18-FY20, activities focused on the creep rupture, fatigue, and creep-fatigue testing of Alloy 709 standard sized ASTM specimens from the first Alloy 709 commercial heat for the short and intermediate term durations. The significant enhancement in the time-dependent mechanical properties, such as the creep property and the creep-fatigue property, of Alloy 709 over

the reference 316H stainless steel is due to the precipitation of nano-sized MX (M=Nb, Ti, X=N, C) or Z-phase (CrNbN) particles on dislocations when the material is in service. However, in low temperature (below 600°C) and low stress conditions, it is concerned that 1) those precipitates are not going to form in a reasonable amount of time due to the slow kinetics, and 2) different types of precipitates, such as the intermetallic laves phase which is believed to be detrimental to creep properties, will be formed preferably over MX or Z-phase. As a result, in FY19, activities was focused on developing an age-hardening heat treatment plan, aiming at bringing out the desired nano-sized precipitates, such as MX or Z-phase, on dislocations, for improved mechanical performance in low stress, low temperature conditions (Zhang, et al. 2019). 775°C/10 h age-hardening treatment was selected as the protocol. In FY20, the treatment was applied to the ESR-1150°C material, and the microstructure was compared with that of the ESR-1100°C material. The effect of solution annealing temperature was determined. A creep-ruptured sample was also studied by investigating specimens from the grip section and from the gauge section. The effect of stress on precipitation was determined.

2 Materials and Methods

U.S. Department of Energy, Office of Nuclear Energy's Advanced Reactor Technologies Program is conducting R&D on qualifying an advanced austenite stainless steel, Alloy 709, for ASME Section III Division 5 constructions in support of development and deployment of sodium fast reactors.

The product chemistry of the first commercial heat conforms to the ranges or maximum values specified in wt.% in Table 2-1. The chemistry aims and the actual melt compositions are also shown in the table.

Table 2-1. Chemical composition of melt of Alloy 709 heat # 58776 (in wt.%)

Alloy 709	C	Cr	Ni	Mn	Mo	N	Si	P	Ti	Nb	B	Fe
Specification range	0.04-0.10	19.5-23	23-26	1.5	1.0-2.0	0.14-0.16	1.0	<0.025	0.2	0.1-0.4	0.002-0.01	Bal
Aim	0.07	20	25	0.9	1.5	0.15	0.40	*	0.05	0.25	0.002-0.005	Bal
Actual	0.066	19.93	24.98	0.91	1.51	0.148	0.44	0.014	0.04	0.26	0.0045	Bal

*The P shall not exceed 0.025 wt.%.

The melt procedure involved three different processing conditions, namely, Argon-Oxygen-Decarburization (AOD), Electroslag Remelting (ESR), and Electroslag Remelting with subsequent homogenization (ESR-Homo). Material slags from those three melting conditions were rolled into 1.1"-1.2" plates. Subsequently, those plates were solution annealed at 1050°C (75 minutes), 1100°C (75 minutes), and 1150°C (60 minutes), respectively. In total, 9 material conditions were obtained. In FY18 scoping test program, it is determined that ESR-1100°C has the best overall mechanical performance, and is therefore carried down for the ASTM code case. In FY20, it was found that after age-hardening at 775°C/10 h, the ESR-1150°C material has better performance than the ESR-1100°C material.

The heat treatment of the ESR-1150°C plate was performed at the central shops of Argonne National Laboratory (ANL) using a vacuum furnace. The plate has a dimension of 24.5" × 15" × 1.1". The heating and cooling was done in vacuum at nominally 2×10^{-6} Torr. Two thermocouples, located near the center of the plate, was used to monitor the temperature. Detailed recording of the heat treatment procedure is attached in the Appendix.

A small piece from the heat treated plate was mechanically polished down to 100 μm in thickness, and 3 mm disks were punched out. The disks were then jet-polished until electron transparent with an electrolyte of 5% perchloric acid and 95% methanol at −30 °C with a Struers TenuPol-5 jet polisher. The microstructures of the TEM samples were characterized using an FEI Talos F200X TEM/STEM at the Center for Nanoscale Materials at ANL. The operating voltage was 200 kV, and the imaging was done in both bright field (BF) and high-angle annular dark-field (HAADF). The instrument was also equipped with a Super X-energy-dispersive spectrometer (EDS) for elemental mapping.

3 Microstructure of age-hardened ESR-1150°C material

Figure 3-1 shows the microstructure of the ESR-1100°C and the ESR-1150°C materials at lower magnifications. It is seen that the 1150° SA dramatically reduced the dislocation density. As dislocations are the preferred nucleation sites for precipitates, it is seen that the overall precipitate density is much lower in the ESR-1150°C material than in the ESR-1100°C material.

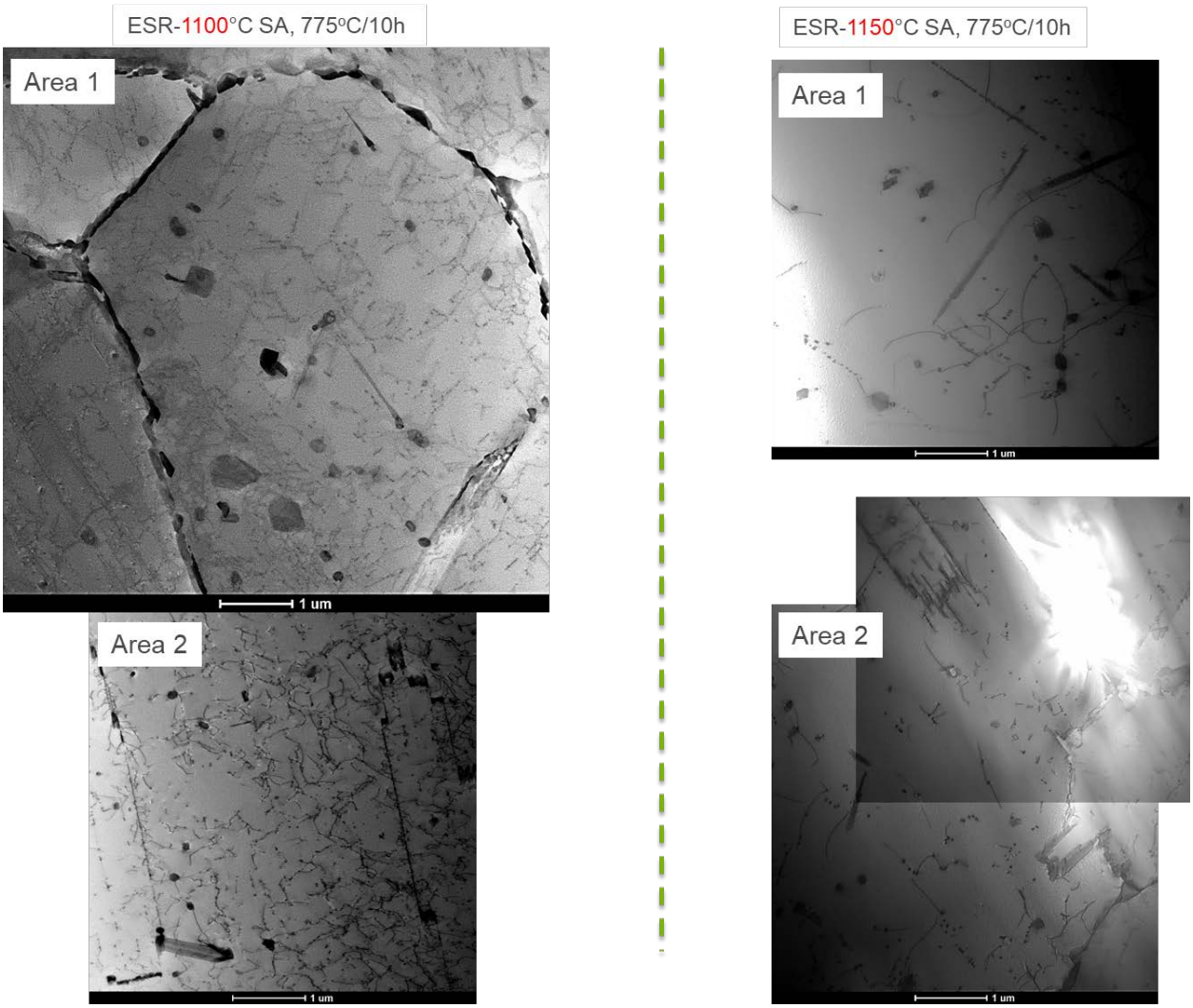

Figure 3-1. TEM-BF images showing the microstructures of the ESR-1100°C and the ESR-1150°C materials at low magnification.

Figure 3-2 shows the major precipitate types in the age-hardened ESR-1150°C material. The grain boundaries are decorated with $M_{23}C_6$ (M = Cr, with substitutions from Ni, Mo and Fe) precipitates. Within a grain, $M_{23}C_6$ preferably grows on residual (undissolved) MX particles, and in some cases, grow into long, needle-like shapes. The dislocations are decorated with fine Nb-rich precipitates smaller than 10 nm, most likely being the MX phase. Figure 3-3 shows the high magnification image and EDS mapping of the MX precipitates. The precipitate types and locations are very similar to those in the aged ESR-1100°C material.

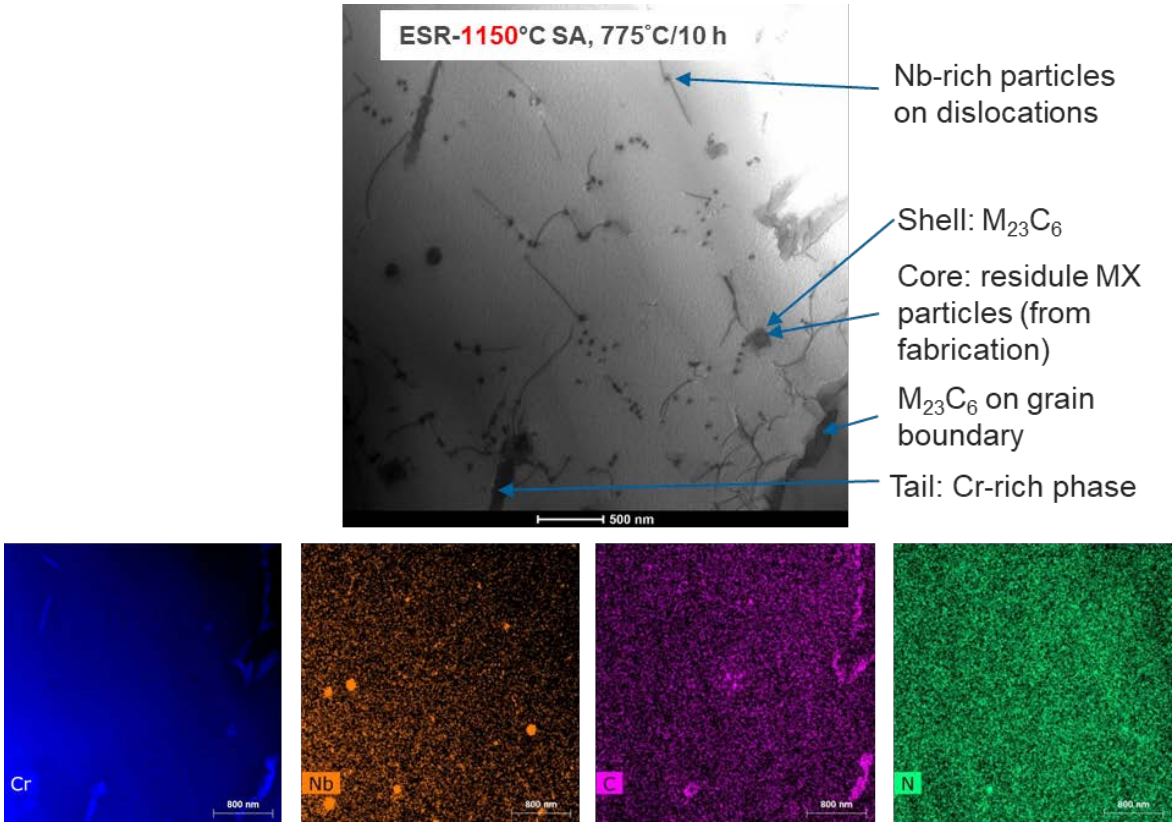

Figure 3-2. Precipitates in 775°C/10 h age-hardened ESR-1150°C material.

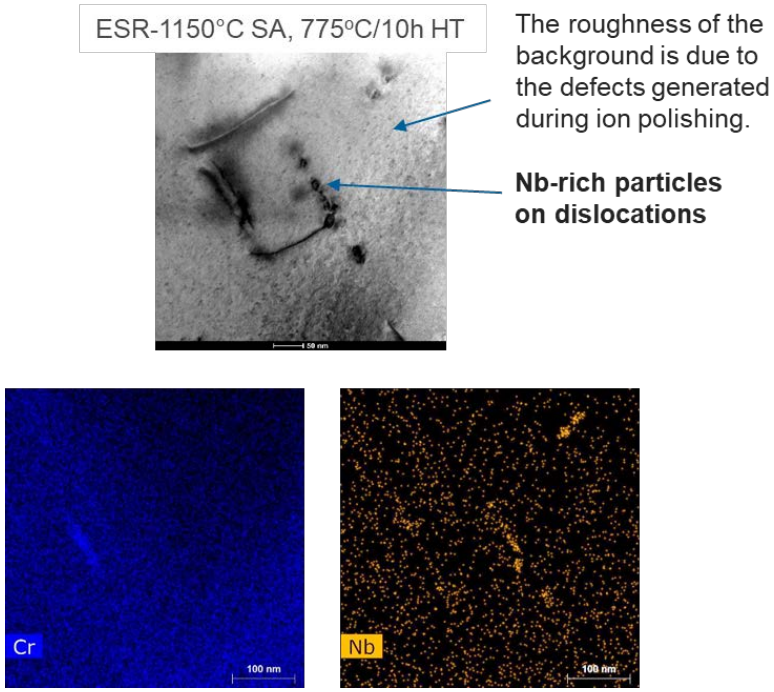

Figure 3-3. High magnification image and EDS mapping showing the nano precipitates on dislocations.

4 Microstructure of a creep-ruptured A709 specimen

The ASTM-standard-sized creep specimen was machined out of an AOD-1100°C plate, with the length direction parallel to the rolling direction, and then creep tested at 600°C/330 MPa to failure. The rupture time was 1752 hours, and the time before the onset of the tertiary creep was ~ 1000 hours. The 3mm-disk TEM samples used in this study were prepared from different regions on the creep-ruptured specimen, as illustrated in Figure 4-1: one from the gauge region but away from the necking center (the gauge sample), containing the creep damage, and one from the grip region (the grip sample), effectively being annealed at 600°C under very low stress for 1754 hours (1752 hours of creep test time plus 2 hours of soaking time before the test started). One untested sample (the as-received sample) was also prepared from the original plate, serving as the control sample.

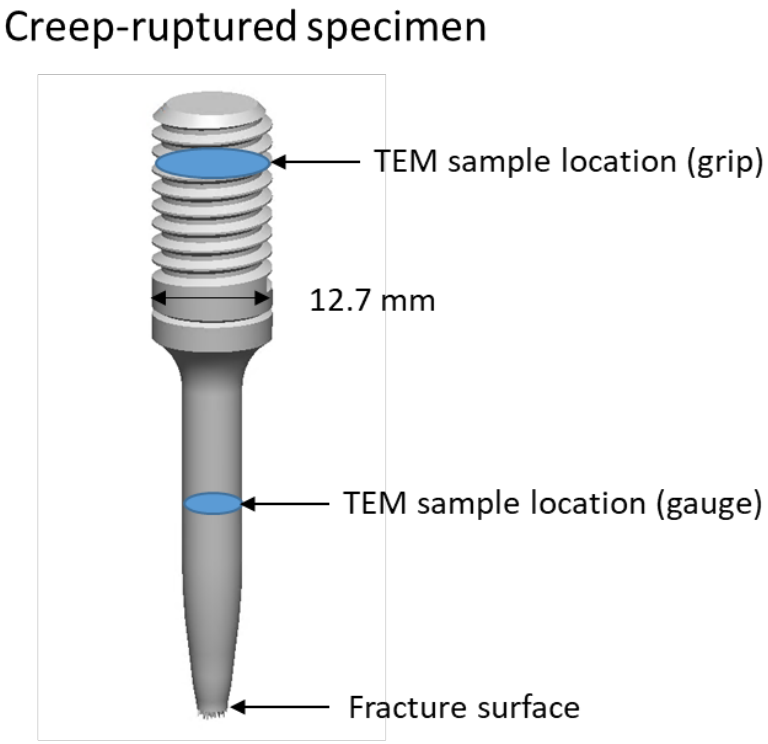

Figure 4-1. A schematic showing the locations on the creep-ruptured sample that the locations from which the TEM samples were prepared.

The sectioned slices from creep-ruptured specimen and as-received material were mechanically polished down to 100 μm in thickness, and 3 mm disks were punched out. The disks were then jet-polished until electron transparent with an electrolyte of 5% perchloric acid and 95% methanol at −30 °C with a Struers TenuPol-5 jet polisher.

Figure 4-2 shows the microstructure of the as-received A709 SS sample. The material exhibits a rather high dislocation density at an average of $3\times10^{13}/m^{-2}$, estimated from a number of TEM images from different locations. Residual (undissolved) MX particles, ranging from 100 nm

to 300 nm, are visible in the TEM image and are confirmed by the EDS mapping. The MX particles are often surrounded by tangled dislocations.

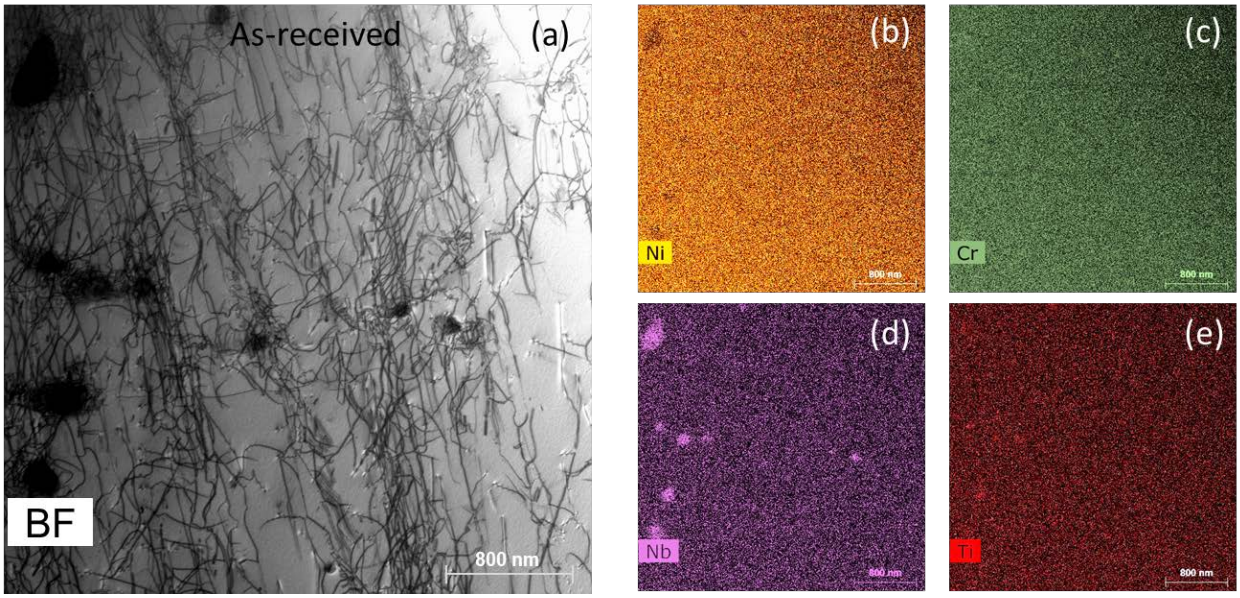

Figure 4-2. Microstructure of the as-received A709 SS sample: (a) TEM-BF image; (b)-(e) EDS elemental maps.

Figure 4-3, Figure 4-4 and Figure 4-5 show the microstructure of the grip sample. As mentioned in Section 2, the sample was effectively annealed for 1754 hours at 600°C. At grain boundaries (upper corners in Figure 4-3 (a)), $M_{23}C_6$ precipitated out, a common observation in stainless steels (Sourmail, T, 2001). Within a grain, needle-like Cr-rich precipitates, likely to be $M_{23}C_6$, are observed at about 10-50 nm wide and several micrometers long, aligning in special crystallographic orientations. Some of the needles have an obvious concentration of carbon in EDS map (Figure 4-3 (i)), while others are not so distinguishable (Figure 4-3 (i) and Figure 4-4 (i)), probably due to the different depth that they are located relative to the sample surface for the carbon signal to be picked up. The needles often grew from residual MX particles by first forming a $M_{23}C_6$ "plate" around the MX particle, and then extending out in a particular direction, as shown in Figure 4-5. The formation of the $M_{23}C_6$ plates around undissolved MX particles in aged austenitic SSs has been reported and explained in literature (Sasmal B, 1997). The formation of the needle is likely to be facilitated by the thickening of a stringers of $M_{23}C_6$ cuboids, as implied by the top needle in Figure 4-5 (a) and the two in Figure 4-5 (b). The mechanism for the formation of stringers has been discussed in (Beckitt, F.R, et al, 1967), the key being the creation of dislocations due to the volume change from the formation of the carbide, which serves as the site for the nuclei of a new carbide aligning in the <110> matrix direction.

Existing line dislocations are also preferred precipitation sites for $M_{23}C_6$ cuboids, as shown in Figure 4-3 and Figure 4-4. Such a phenomenon has been reported in literatures in aged austenitic SS (Beckitt, F.R, et al, 1967). This observation also proves that different from the 775°C/10 h aging condition (Figure 3-2, Figure 3-3), at 600°C temperature regime or lower, the MX phase does not precipitate out on dislocations, but rather the $M_{23}C_6$ phase.

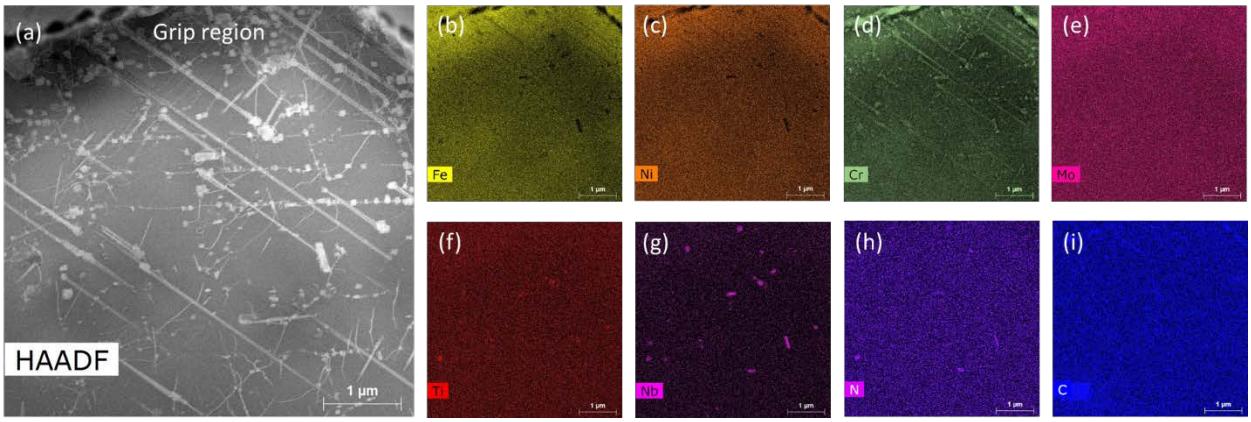

Figure 4-3. Microstructure of the grip sample: (a) STEM-HAADF image; (b)-(i) EDS elemental maps.

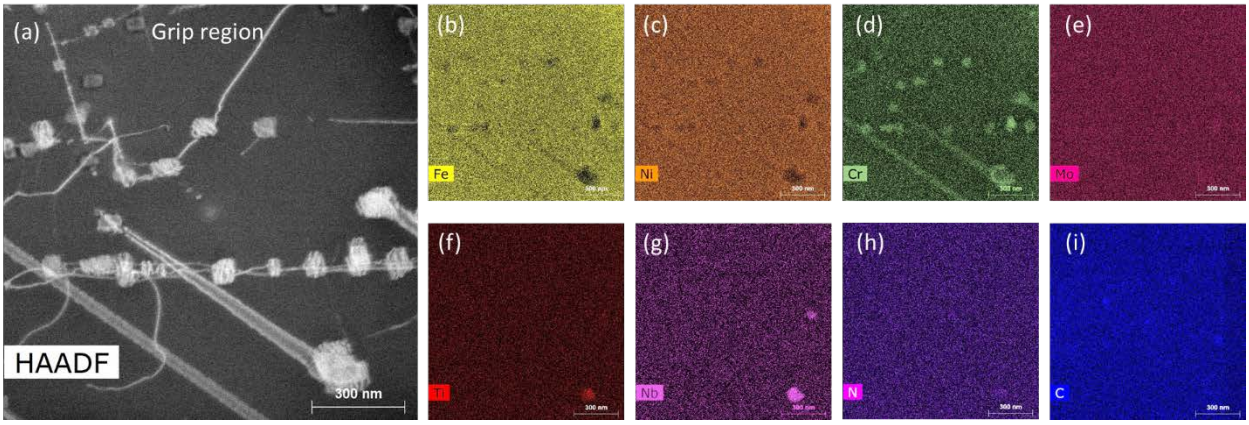

Figure 4-4. Microstructure of the grip sample, showing the $M_{23}C_6$ cuboids on dislocations: (a) STEM-HAADF image; (b)-(i) EDS elemental maps.

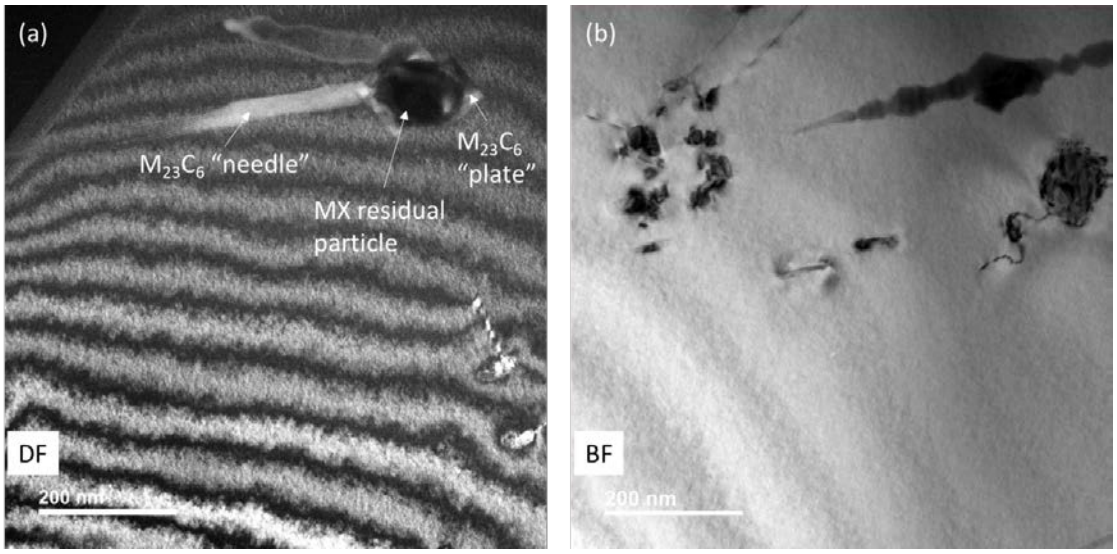

Figure 4-5. Microstructure of the grip sample: (a) TEM-DF image showing an area with needle-like $M_{23}C_6$ precipitates; (b) TEM-BF image showing another area with needle-like $M_{23}C_6$ precipitates. Both images were taken near [110]-zone, using (200)-g at g-4g condition.

Figure 4-6, Figure 4-7 and Figure 4-8 show the microstructure of the gauge sample. Large area views in Figure 4-6 reveal that the sample contains very high densities of dislocations and precipitates. No needle-like precipitates are observed. The EDS maps in Figure 4-7 show that the large precipitates are all enriched in Cr and Mo, some of which are also enriched in Si. According to literature studies (Sourmail, T, 2001), the Si-rich phase is Cr_3Ni_2SiX and the other is $M_{23}C_6$. Figure 4-8 shows that on dislocations, ultrafine Nb-rich precipitates form with sizes smaller than 10 nm. Those precipitates, likely to be MX, form during the creep test and give the high creep resistance of the material by increasing the strength and pinning the dislocation motion.

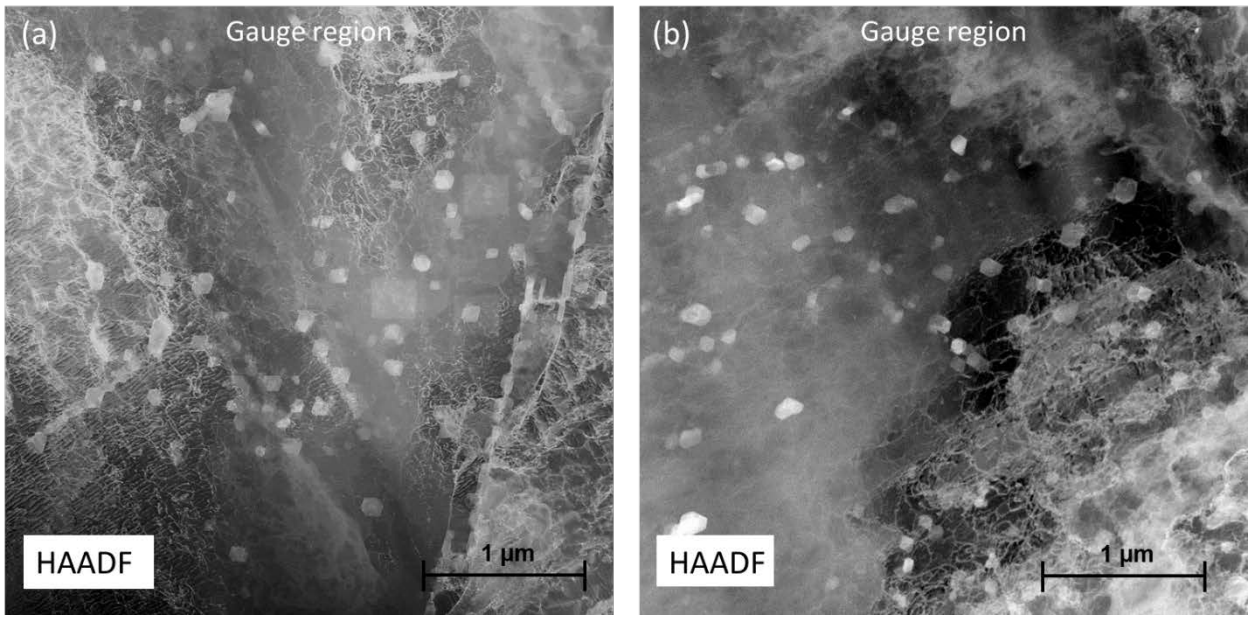

Figure 4-6. STEM-HAADF images showing the microstructure of the gauge sample.

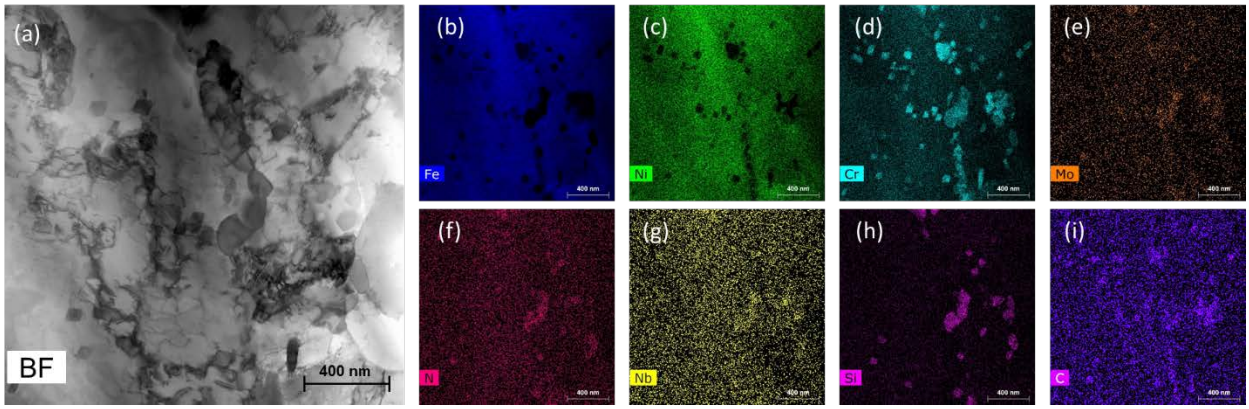

Figure 4-7. Microstructure of the gauge sample: (a) STEM-BF image; (b)-(i) EDS elemental maps.

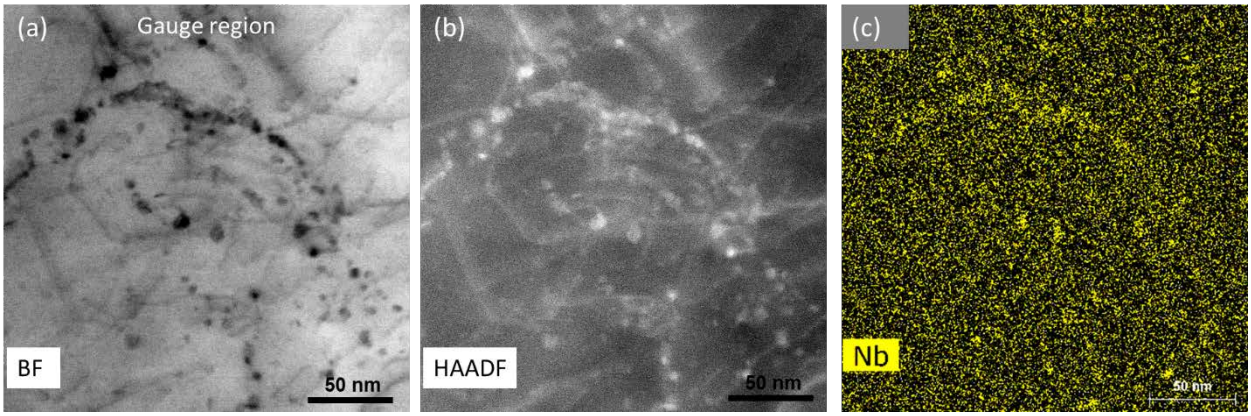

Figure 4-8. Microstructure of the gauge sample, showing the Nb-rich (presumbly MX) precipitates on dislocations: (a) STEM-BF image; (b) STEM-HAADF image. (c) EDS Nb map.

Discussion

Age hardening brings out the solutes from the matrix and forms precipitates. Compared to the ESR-1100°C material, the ESR-1150°C material has less dislocation density, hence less MX precipitate density from 775°C/10 h aging (Figure 3-1). This implies that there are more Nb atoms in solution in the aged ESR-1150°C material. The MX precipitates on existing dislocations pin the dislocation motion, which is the desired mechanism to achieve enhanced creep properties. However, under low temperature (<600°C), low stress service conditions, those precipitates will not be able to form due to the slow kinetics. Having the material age hardened using the protocol in this study (775°C/10 h) to bring out the nano precipitates on dislocations should enhance the creep performance of the Alloy 709 under low temperature, low stress conditions. At higher temperature conditions, the remaining Nb solutes in the matrix will be able to precipitate out in-service to even more effectively pin the dislocations.

The study of the grip region and the gauge region of the creep-ruptured sample revealed the importance of stress on precipitation. At the same temperature, the creep stress dramatically increased the dislocation density, changed the precipitate types, and changed the precipitate morphology. The potentially detrimental, needle-like $M_{23}C_6$ precipitates, due to their brittleness to lead to ductility reduction [R. Ding et. al. Mat. Des. 2019], do not form in stressed condition. The stress facilitates the participation of Si in precipitation, leading to the formation of Cr_3Ni_2SiX. The stress also facilitates the diffusion of Nb, leading to the precipitation of the MX phase on dislocations rather than the $M_{23}C_6$ phase. The study of the creep-ruptured sample leads to the conclusion that in evaluating a materials performance, it is important to take the environmental factors into account.

Summary and Future Work

Age-hardening at 775°C/10 h of the commercial heat of A709 ESR-1150°C was studied aiming at improving the creep performance of the material. TEM/STEM characterization were performed. It was observed that solution annealing at 1150°C dramatically reduced the dislocation densities compared to the 1100°C solution annealing, leading to a much lower precipitate density since dislocations were the preferred nucleation sites of the MX phase. M23C6 precipitated on grain boundaries and within grain interior, preferably on residual (undissolved) MX particles. The implication on mechanical properties was discussed, and it was concluded that the heat treatment was beneficial to the creep performance, especially at low temperature, low stress conditions.

Microstructures from the grip region and from the gauge region of a 600°C/330 MPa creep-ruptured sample were studied by TEM/STEM. The precipitate types, morphologies and densities were very different from those different regions. Such observations emphasized the importance of the environmental factors, such as stress, on the microstructural response of materials.

Future work involves the microstructural characterization of a variety of different types of deformed samples, including fatigued, creep-fatigued, and crept, from age-hardened or not age-hardened materials. Such a study will help to elucidate the role of precipitation in mechanical deformation. In addition, in FY21 and FY22, synchrotron x-ray beamtime will be allocated at the Advanced Photon Source for in-situ x-ray diffraction study of deformation processes in A709. Such state-of-art experiments will greatly enhance the understanding of the microstructure-property correlation in A709.

Acknowledgement

Programmatic direction was provided by the Office of Nuclear Reactor Deployment of the Office of Nuclear Energy.

The authors gratefully acknowledge the support provided by Sue Lesica, Federal Manager, Advanced Materials, Advanced Reactor Technologies (ART) Program, Brian Robinson, Federal Manager, ART Fast Reactors (FR) Campaign, and Robert Hill of Argonne National Laboratory, National Technical Director, ART FR Campaign.

The authors acknowledge the assistance of D. L. Rink for specimen preparation.

This research used resources of the Center for Nanoscale Materials, a U.S. Department of Energy (DOE) Office of Science User Facility operated for the DOE Office of Science by Argonne National Laboratory under Contract No. DE-AC02-06CH11357.

References

Busby, J. T., S. Byun, R. Klueh, P. Maziasz, and J. Vitek, K. Natesan, M. Li, R. Wright, S. Maloy, M. Toloczko, A. Motta, B. D. Wirth, G. R. Odette, and T. Allen, "Candidate Developmental Alloys for Improved Structural Materials for Advanced Fast Reactors," ORNL/GNEP/LTR-2008-023, March 2008.

Natesan, K., X. Zhang, T.-L. Sham, and H. Wang, Argonne National Laboratory Report, ANL-ART-89, June 2017.

Zhang, X, T.-L Sham, G. A. Young, Argonne National Laboratory Report, ANL-ART-170, August 2019.

Sourmail, T, Materials Science and Technology, 17 (2001)

Sasmal B., Journal of Materials Science, 32 (1997)

Beckitt, F.R., B.R. Clark, Acta Metallurgica 15 (1967)

Li, M, W.Y. Chen, X. Zhang, K. Natesan, Argonne National Laboratory Report, ANL-ART-135, September 2018.

Ding R., J. Yan, H. Li, S. Yu, A. Rabiei, and P. Bowen, Mater. Des. 176 107843 (2019)

Appendix

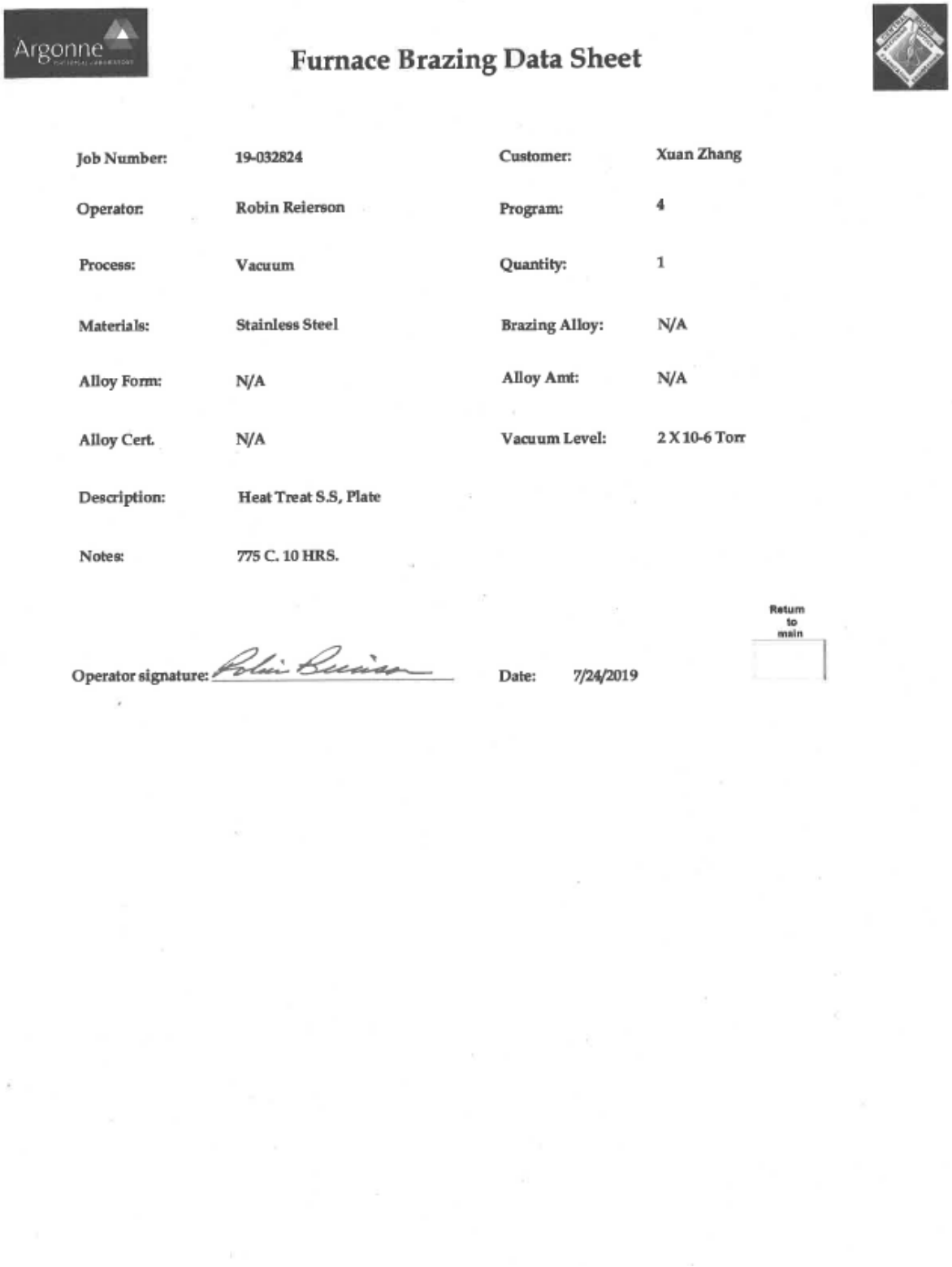

Argonne

Furnace Brazing Data Sheet

Job Number:	19-032824	Customer:	Xuan Zhang
Operator:	Robin Reierson	Program:	4
Process:	Vacuum	Quantity:	1
Materials:	Stainless Steel	Brazing Alloy:	N/A
Alloy Form:	N/A	Alloy Amt:	N/A
Alloy Cert.	N/A	Vacuum Level:	2 X 10-6 Torr
Description:	Heat Treat S.S, Plate		
Notes:	775 C. 10 HRS.		

Return to main

Operator signature: Robin Reierson Date: 7/24/2019

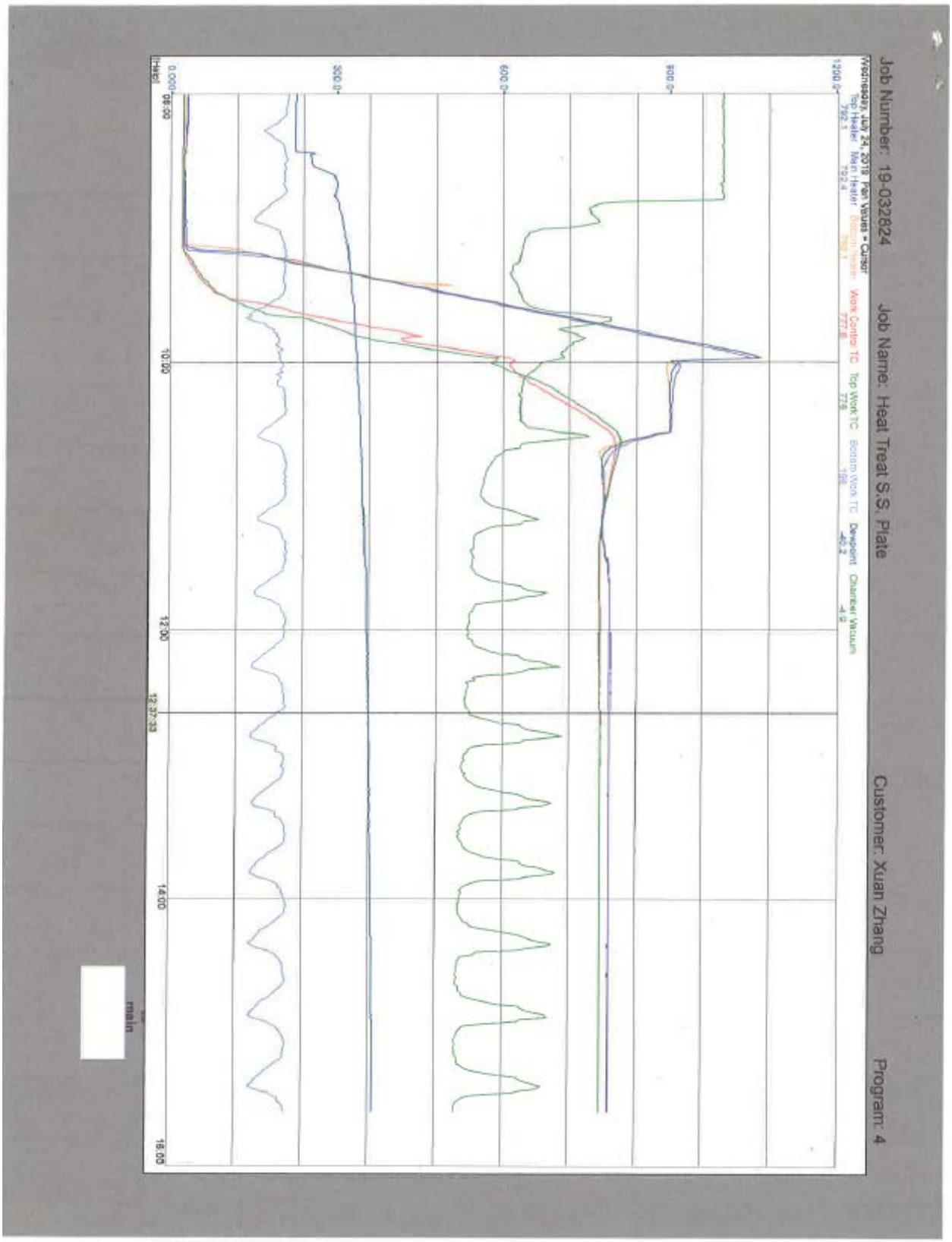
Job Number: 19-032824
Job Name: Heat Treat S.S. Plate
Customer: Xuan Zhang
Program: 4
Wednesday, July 24, 2019 Plot Values = Cursor
Top Heater
Mast Heater
Bottom Heater
Work Control TC
Top Work TC
Bottom Work TC
Dewpoint
Chamber Vacuum
792.4
777.6
776
-40.2
-4.9
1200.0
900.0
600.0
300.0
0.000
Hrs:
08:59
10:00
12:00
12:37:33
14:00
16:00
main

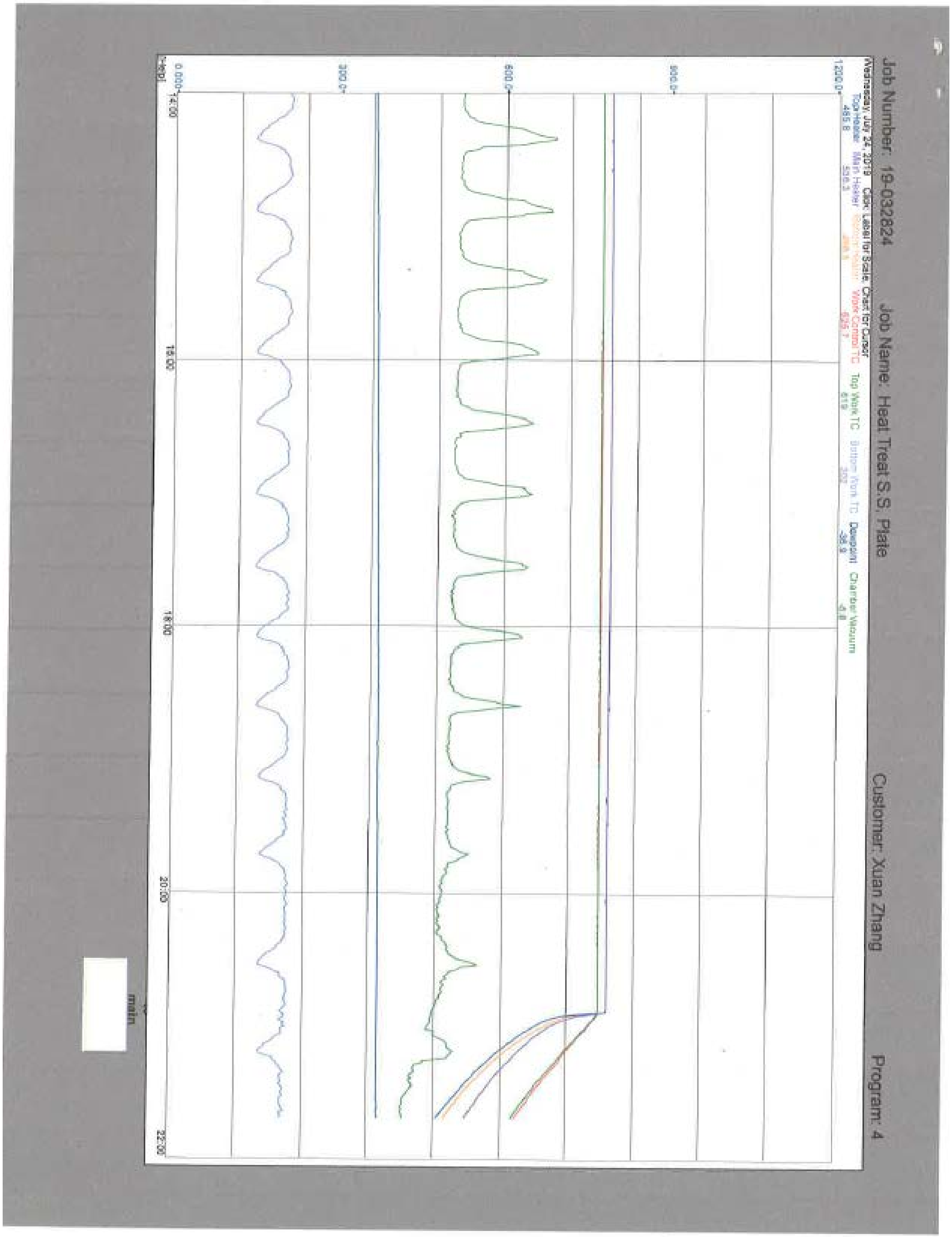
Job Number: 19-032824
Job Name: Heat Treat S.S. Plate
Customer: Xuan Zhang
Program: 4
Wednesday, July 24, 2019 Click Label for Scale, Chart for Cursor
Top Heater
Main Heater
Work Control TC
Top Work TC
Bottom Work TC
Dewpoint
Chamber Vacuum
1200.0
900.0
600.0
300.0
0.000
14:00
16:00
18:00
20:00
22:00
main

Locations of thermocouples on the A709 plate during aging:

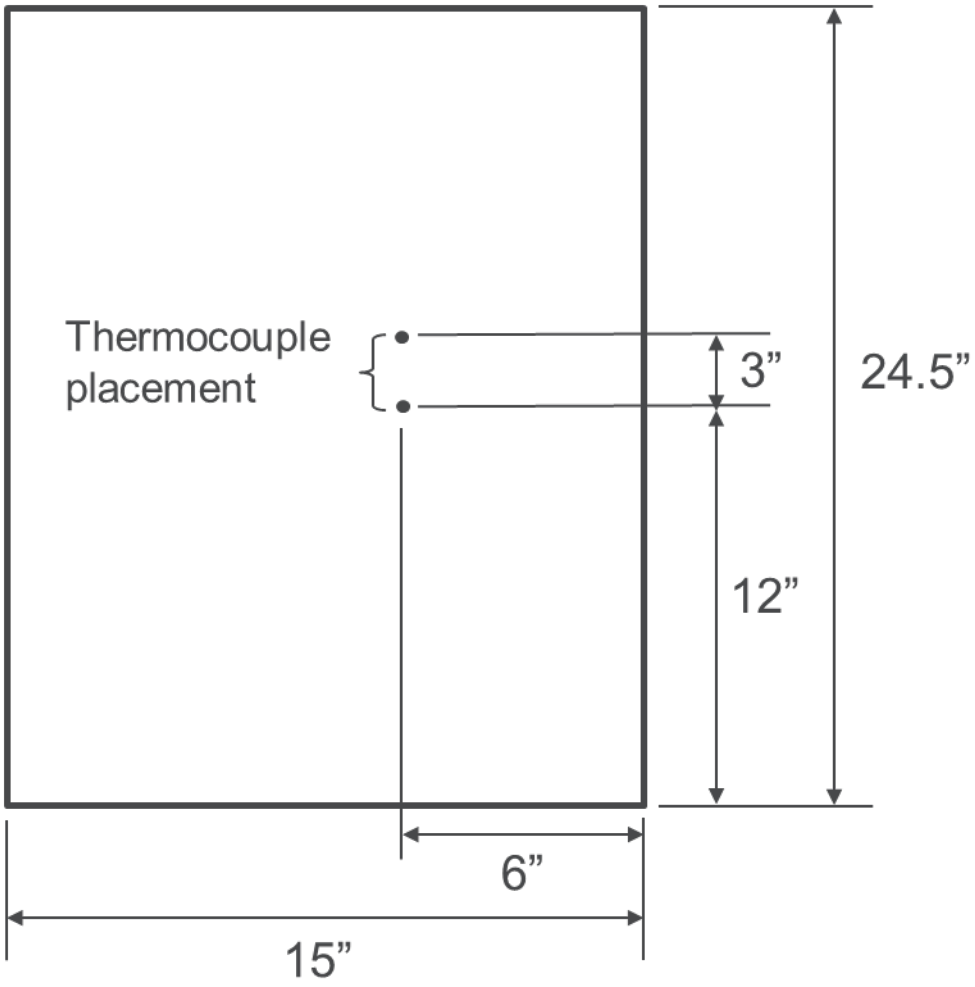

Applied Materials Division

Argonne National Laboratory

9700 South Case Avenue

Argonne, IL 60439

www.anl.gov